Progress in PIV-PTV methods: application to concentration measurements

A.Stitou, M.L. Riethmuller

e-mail: stitou@vki.ac.be

von Karman Institute for Fluid Dynamics (VKI)
chaussée de Waterloo, 72
1640 Rhode-Saint-Genèse
Belgium

Abstract

The purpose of this work is to discuss the ability to simultaneously measure the concentration of dispersed particle and the velocity field. It is basically an extension of particle imaging methods (such as PIV or PTV). These methods experienced major developments during this last decade and became nowadays very common instruments. Such combined tool would be valuable for investigating the distribution of droplet in combustion, the dispersion of pollutant gas or other similar applications.

The main idea consists to use all the information available on the image to measure the concentration. Image processing provides an instantaneous velocity field for each couple of images and analyzing the spatial distribution of the particle images gives simultaneously a concentration field. A method based on particle counting is investigated and characterized.

It is showed that trade-off has to be made between the accuracy and the spatial resolution. Systematic tests on synthetic images and real images showed that the tool has a non-linear response. Nevertheless, the mean measurements present self-similar profile and a correction is possible if experimental parameter such as particle image diameter are determined. The instantaneous measurements are more delicate. They present scatter due to the performances of identification algorithm and due to the error made on the particle position.

1.Introduction

Simultaneous measurement of velocity and concentration field is a challenging task in many applications: droplet in combustion, the dispersion of pollutant gas… Therefore, one has to turn towards advanced experimental techniques such as PIV-LIF to investigate such flow fields. This work proposes an alternative method that is an extension of classical particle imaging methods (such as PIV or PTV) and focuses on the investigation of dispersion of particle.

The main idea consists to use all the information available on the image to measure the concentration. Therefore, the set-up required is exactly the same that is used for PIV-PTV measurement as depicted in figure 1. It is simpler and need less equipment and settings than techniques used for similar purposes such as PIV-LIF (refer e.g. to Westerweel, 2000). It presents also the advantage to be applicable for airflows. The flow of interest is seeded with particle. Then, the region to be investigated is illuminated by a powerful light source (typically a pulsed laser) and images are recorded. The particles embedded in the flow act as tracer for the velocity measurement but also for the concentration one. Hence, image processing provides an instantaneous velocity field for each couple of images and analyzing the spatial distribution of the particle images gives simultaneously a concentration field.

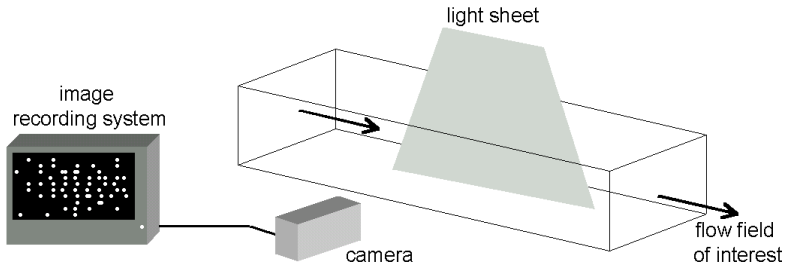

Figure 1: set-up for concentration measurement

By this method, we only access to a planar measurement. The concentration is then expressed in particle by surface area (1/pixel^2 or 1/m^2). Volume concentration can be obtained assuming uniformity along the light sheet thickness (L_t):

$$C_{3D} = \frac{C_{2D}}{L_t}$$

Derived quantities (mass and volume concentration) can also be defined but the most interesting quantity is the relative concentration:

$C_m = C \,.\, M_p$ with: M_p mass of a particle
$C_v = C \,.\, V_p$ V_p volume of a particle

2.Identification algorithm

Before analyzing the spatial distribution of the particle images, an identification and localization process has to be performed on the recorded frames. The extraction of particles from recorded images is a critical task and constitutes in itself a general problem in pattern recognition research. It seems that there is no universal method and specific approaches have to be considered for any particular application. Several authors have discussed this topic in different ways Carosone et al. (1995), Etoh et al. (1998), Guezennec and Kiritsis (1990)…). Nevertheless, this task can become easier and the performances will be improved if one spends some times optimizing the experimental conditions and performs image acquisition more carefully.

The method used in this work was initially developed for images obtained for classical PIV. The extraction of the particle image is performed according to the algorithm proposed previously by the authors (Stitou and Riethmuller, 2001). The method is based on the determination of a local intensity threshold using reference images in order to determine the background noise (figure 2). If reference images are not available, it is also possible to analyze the distribution of the gray levels by dividing the whole image in smaller regions and applying the thresholding method of Guezennec and Kiritsis (1990)… A double gaussian interpolation is then performed to get to the position at the sub-pixel accuracy.

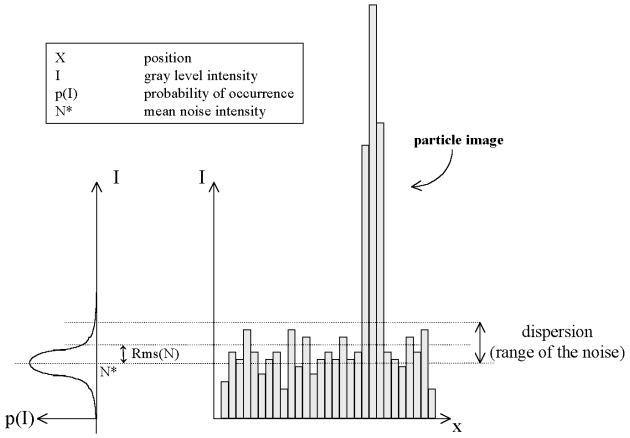

fig 2: particle image detection method

3. Concentration measurement by counting

3.1.Principle

This approach to measure the spatial distribution of the seeded particle is summarized in figure 3. After processing the recorded images, the local concentration (C_m) is measured by counting particle ($\#_d$) lying inside an interrogation area of interest (S_w) and it is defined as:

$$C_m = \frac{\#_d}{S_w}$$

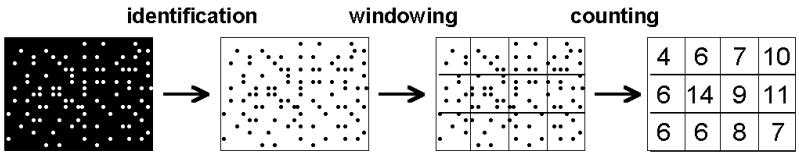

Figure 3: concentration measurement by counting

It can be represented by the following mathematical operator:

$$C_w = \frac{\iint_w \left(\sum_p \delta(x - x_p, y - y_p) \right) dS}{\iint_w dS}$$

with: w window of interest
(x_p,y_p) particle image position
$\delta(x)$ Dirac function

3.2.Effect of the pixelisation on the dynamic range

Theoretical limitations are discussed. The dynamic range refers to the number of concentration levels that can be measured. As a matter of fact, due to the pixelisation of the recorded images, measurements based on particle identification are therefore of a discrete nature. The theoretical performances are bounded by the ideal case where a particle can be identified at each pixel. Intermediate situation described in figure 4 are also considered if a particle is identified using a peak finding strategy.

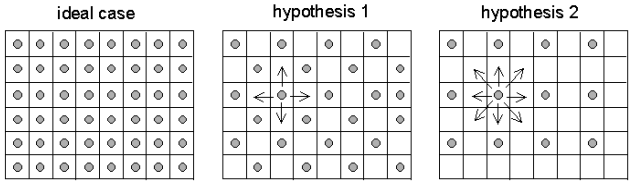

Fig 4: pixelisation effect (dots represents a identified particle image)

The dynamic range and the maximum measurable concentration can be computed easily. A plot is presented on figure 5 and figure 6 (for square interrogation areas).

	#levels	max(C_m) ($1/pix^2$)	resolution ($1/pix^2$)	resolution/max(C_m)
ideal case	w_s^2	1	$1/w_s^2$	$1/w_s^2$
hypothesis 1	(1/2). w_s^2	0.5	$1/w_s^2$	$2/ w_s^2$
hypothesis 2	(1/4). w_s^2	0.25	$1/w_s^2$	$4/ w_s^2$

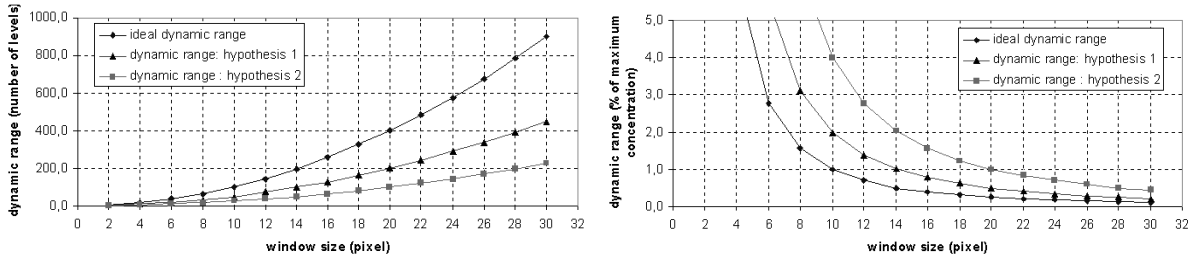

Fig 5: theoretical dynamic range of the counting method

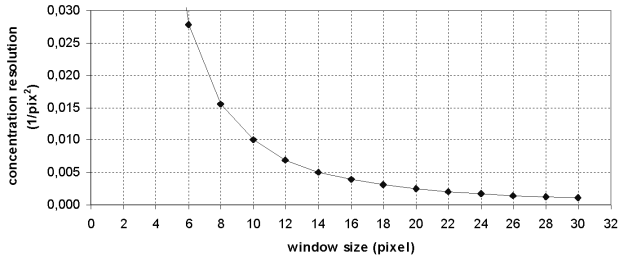

Fig 6: theoretical concentration resolution of the counting method

Hence, a trade-off between the spatial resolution (related to the interrogation window size) and the accuracy has to be made.

3.3. Effect of the extraction of the image of the tracers

The ability to identify a particle image is also the source of a measurement scatter. Assuming that all the tracers have the same probability p_d to be detected, the measurement of a constant concentration can be described by a binomial random process. Then, the mean and the standard deviation are calculated for a constant concentration:

$$\overline{N_m} = N_r.p_d \qquad \sigma_{N_m} = \sqrt{N_r.p_d.(1-p_d)}$$

The ratio between the error scatter and the real concentration, plotted in figure 7, is:

$$\frac{\sigma_{C_e}}{C_r} = \frac{\sigma_{N_d}}{N_r} = \frac{1}{w}.\frac{1}{\sqrt{C_r}}.\sqrt{p_d.(1-p_d)}$$

with:
- C_e error on the measured concentration
- C_r real concentration
- w_s interrogation window size
- N_d number of identified particle in the area of interest
- N_r real number of particle present in the area of interest

This simple model can be improved if one considers that the particles are distributed in classes with p_i being the probability based on some characteristics (D_p, I_p…) that a particle of this group is identified or not. We suppose also that there is no correlation between the probabilities associated to each class.

$$\begin{cases} N_m = N_d = \sum_i N_{d,i} \\ N_i = \alpha_i.N_r \end{cases} \rightarrow \begin{cases} \overline{N_m} = \sum_i \overline{N_{d,i}} = \sum_i N_i.p_i \\ \sigma_{N_m} = \sqrt{\sum_i \sigma^2_{N_{d,i}}} = \sqrt{\sum_i N_i.p_i.(1-p_i)} \end{cases} \rightarrow \frac{\sigma_{C_e}}{C_r} = \frac{\sigma_{N_m}}{N_r} = \frac{1}{w_s}.\frac{1}{\sqrt{C_r}}.\sqrt{\sum_i \alpha_i.p_i.(1-p_i)}$$

with:
- $N_{d,i}$ number of identified particle from class i in the area of interest
- α_i fraction of particles of class i

As expected, the scatter decreases when increasing the window size.

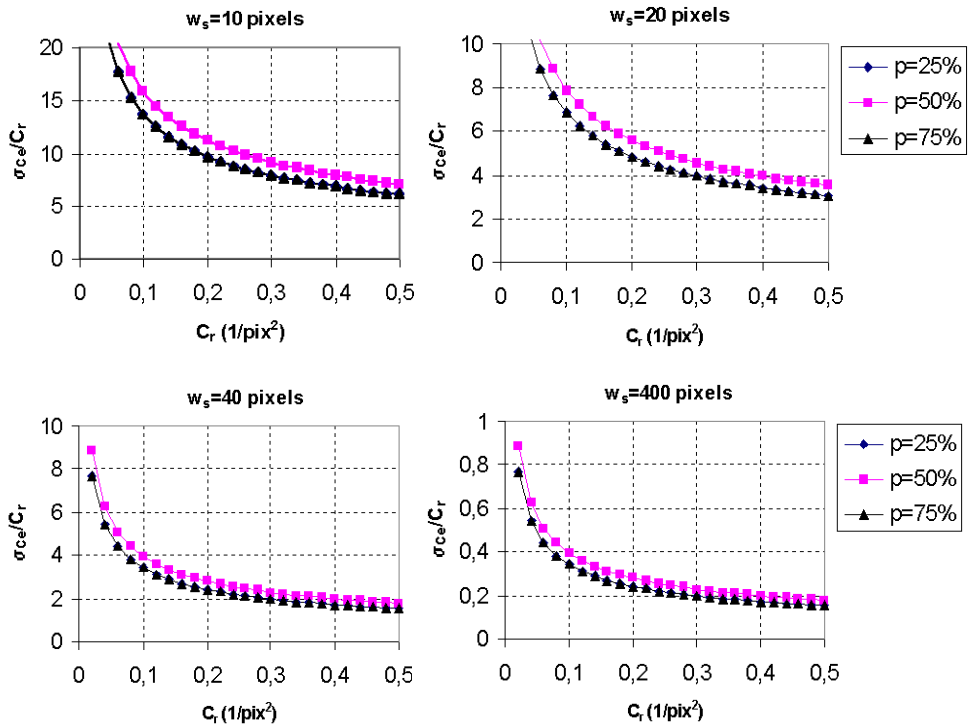

Fig 7: effect of the probability to retrieve a particle image on the scatter of the measurement (simple binomial model)

3.4.Effect of the error on the measurement of particle image position

The error on the measurement of the position of particles (represented by its standard deviation σ_{xe}) is also the source of concentration measurement scattering. As a matter of fact, particle localized at a wrong position can be accounted in another window than the one that it should be. We will assume in the following discussion an ideal situation where the entire particles are identified ($N_d = N_r$).

$$C_m = \frac{1}{w_s^2}.\left(N_d - N_o + \sum_{i \neq w} N_{i \to w}\right) \approx \frac{1}{w_s^2}.\left(N_d - N_o + \left(N_N + N_S + N_E + N_W\right) + \left(N_{NE} + N_{NW} + N_{SE} + N_{SW}\right)\right)$$

with: N_d number of identified particle that are really lying in the window of interest
N_o number of identified particle of the window of interest that are localized outside this area
N_N, N_S, N_W, N_E, N_{NE}, N_{NW}, N_{SW}, N_{SE} number of particle from the neighboring window localized into the window of interest according to figure 8.

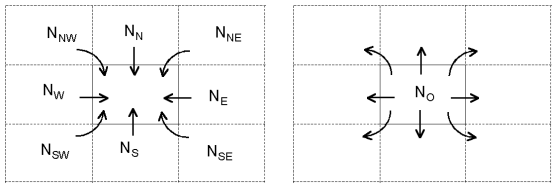

Fig 8: effect of the error on the measurement of particle position

This is the case if we consider only the neighboring window, which is reasonable for $w_s/\sigma_{xe} >> 1$. Computing the mean, it comes:

$$\overline{C_e} = \overline{C_m} - C_r = \frac{1}{w_s^2}.\left(-\overline{N_o} + \left(\overline{N_N} + \overline{N_S} + \overline{N_E} + \overline{N_W}\right) + \left(\overline{N_{NE}} + \overline{N_{NW}} + \overline{N_{SE}} + \overline{N_{SW}}\right)\right)$$

But the average number of particle "moving" outside a window of interest is the same than the one that is entering. Therefore, the error σ_{xe} doesn't affect the mean concentration measurement and then no more bias is introduced. Considering the variance (and the standard deviation), a scatter is added to the ideal situation. We assume that the random variable N_o ,N_N, N_S, N_W, N_E, N_{NE}, N_{NW}, N_{SW}, N_S are non-correlated binomial processes

characterized respectively by p_{out}, p_{side} and p_{corner}. Their calculations are done in annex 1 and annex 2. It comes out that the probability that a particle is localized in the wrong window is only function of w_s/σ_{xe}. The relative error can be expressed as:

$$\sigma_{N_m}^2 = \left(\sigma_{N_O}^2 + \left(\sigma_{N_N}^2 + \sigma_{N_S}^2 + \sigma_{N_E}^2 + \sigma_{N_W}^2\right) + \left(\sigma_{N_{NE}}^2 + \sigma_{N_{NW}}^2 + \sigma_{N_{SE}}^2 + \sigma_{N_{SW}}^2\right)\right)$$

$$\rightarrow \quad \frac{\sigma_{C_e}}{C_r} = \frac{\sigma_{N_m}}{N_r} = \frac{1}{w_s}\cdot\frac{1}{\sqrt{C_r}}\cdot\underbrace{\sqrt{p_{out}\cdot(1-p_{out}) + 4\,p_{side}\cdot(1-p_{side}) + 4\,p_{corner}\cdot(1-p_{corner})}}_{f\left(\frac{w_s}{\sigma_{xe}}\right)}$$

3.3.Synthetic images analysis

A systematic analysis of the performances is held using synthetic images. A wide range of seeding condition is considered. The seeding concentration (C_r) is defined as the number of particle images by surface. It is important to note that the results presented here are relative to this detection algorithm and to this interpolation scheme for the position evaluation. 8 bits frames are generated and Mie scattering is assumed leading to gaussian shaped particle image. The intensity of the individual particles is linearly added. The main characteristics are:

- Gaussian laser sheet thickness is simulated with maximum intensity of 50, 66 and 80 % of the saturation level
- Simulated pixel fill ratio = 0.7
- The particle diameter (D_p) is respectively 3, 4 and 5 pixels.
- A constant concentration is ensured in each window. 16000 are generated to achieve statistical convergence.
- No noise is added

The results are showed on figure 9 for the mean measured concentration. It shows that the illumination power doesn't affect the performances. On another hand increasing the particle image diameter keeping a constant concentration makes the measurement more difficult. We observe also that the range of measurable concentration is limited and that the maximum value depends on the particle diameter and on the window size. The effect of the later is due to the pixelisation effect explained previously. The measurement tool has a non-linear response and the sensibility decreases while increasing the concentration.

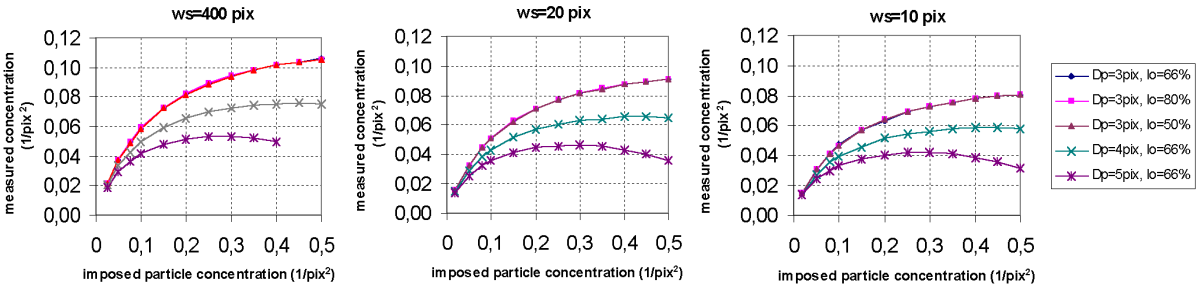

Fig 9: mean concentration measured on synthetic images for constant real concentration

The non-linear behavior is explained looking to figure 10, which shows that the efficiency to detect particle images is decreasing at high concentration levels.

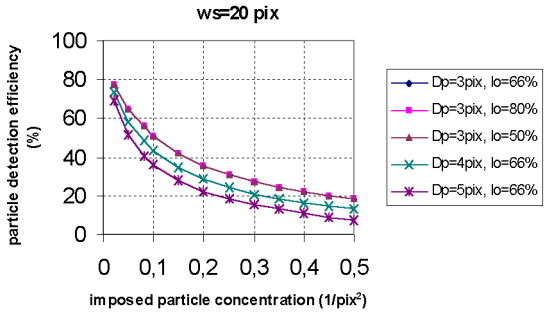

Fig 10: particle detection efficiency on synthetic images

The scatter of the error is also plotted on figure 11. It is observed that the simple binomial model is overestimating the dispersion of the measurements and then a finer modelisation of the processes is needed to get accurate predictions.

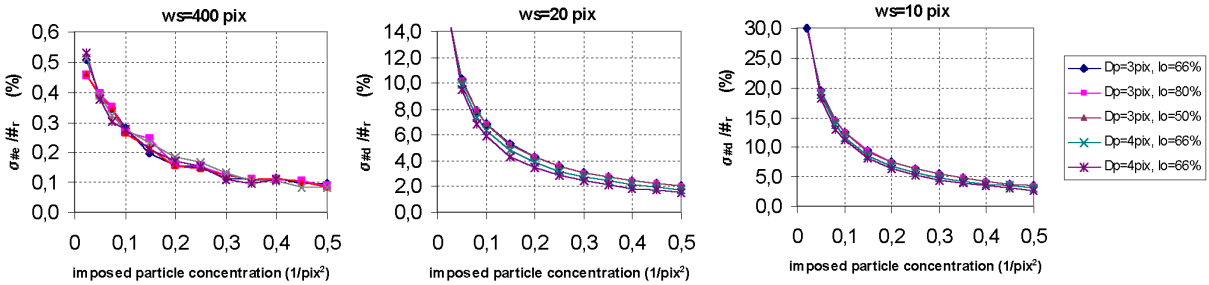

Fig 11: measurement scatter on synthetic images

The averaged measurement are normalized and presented on figure 12. They present self-similar profiles. Hence a correction of the bias due to the non-linear response is possible if one can evaluate the experimental parameters such the particle image diameter. Zimmer et al (1999) proposed to use a simple interpolation scheme to evaluate the size of droplet in sprays. This approach could then be applied for our purpose

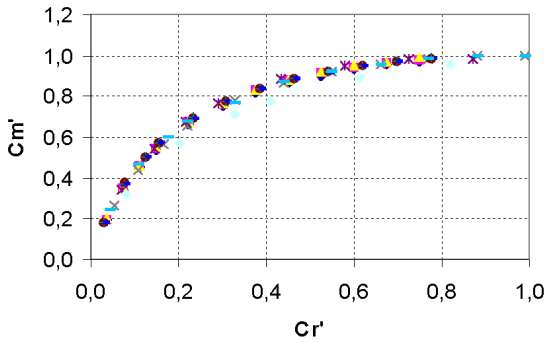

Fig 12: non-dimensional mean concentration measurement on synthetic images

3.4. Test case with real image

For comparison purpose, an experimental test case is considered. A low speed wind tunnel (3.75 m/s) is used. A smoke generator seeds the flow with oil droplets. They are illuminated by a Nd:Yag laser (200 mJ). A new generation camera (PCO Sensicam, CCD sensor of 1280 by 1024 pixel^2) acquires the images. A useful area of 750 by 720 pixel^2 is grabbed. The PIV system is synchronized with a signal generator. In order to evaluate the concentration, the set-up described in figure 13 is adopted. A laser beam of 17 mW crosses the test section. A photo-multiplier is placed in forward scattering mode. These devices are normally designed for LDV measurement. The light intensity scattered by the particles (I) is proportional to their concentration (C_p) and to the square of the diameter (D_p), according to the work of van de Hulst (1957):

$$I = D_p^2 . C_p . k$$

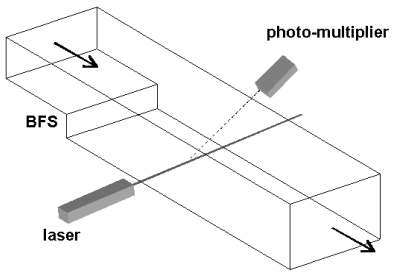

Fig 13: set-up for seeding concentration measurement

Figure 14 depicts some of the acquired images with different seeding concentration. The results after processing the image are presented on figure 15. The trends observed on these images are similar to the one obtained with synthetic images. We should note that the unit representing the concentration of tracer is arbitrary since it is the voltage of the signal delivered by the photo-multiplier. It only gives a relative value.

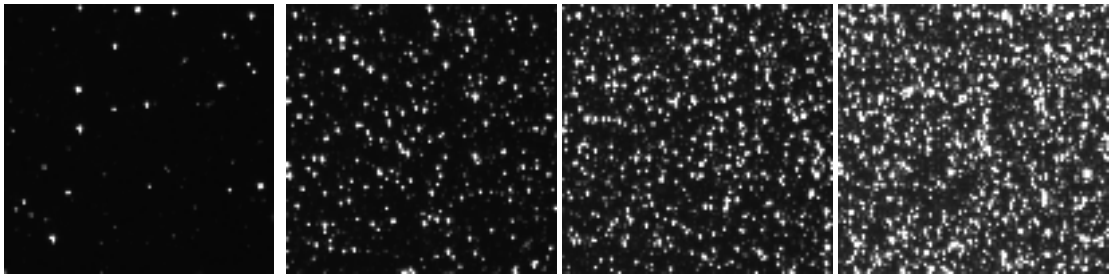

Fig 14: acquired images with different seeding concentration

The measurements are also rescaled in figure 15 in order to get the same non-dimensional presentation than synthetic images. A good agreement is obtained for the mean concentration.

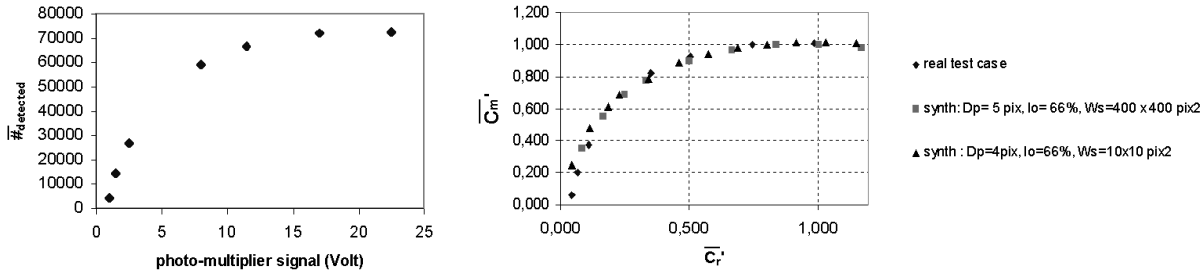

Fig 15: results from a real test case

4. Concentration measurement by triangulation

Another approach is presented on figure 16. Its principle consists in measuring the surface occupied by each particle. The easiest way to achieve this task is to perform a triangulation. The Delaunay method is generalized in the CFD world and its properties are very well known. The measured concentration is then:

$$C_p = \frac{1}{S_p} = \frac{1}{\sum_t \frac{S_{p,t}}{3}}$$

with: S_p surface occupied by a particle image
$S_{p,t}$ surface of a triangle with the particle as vertex

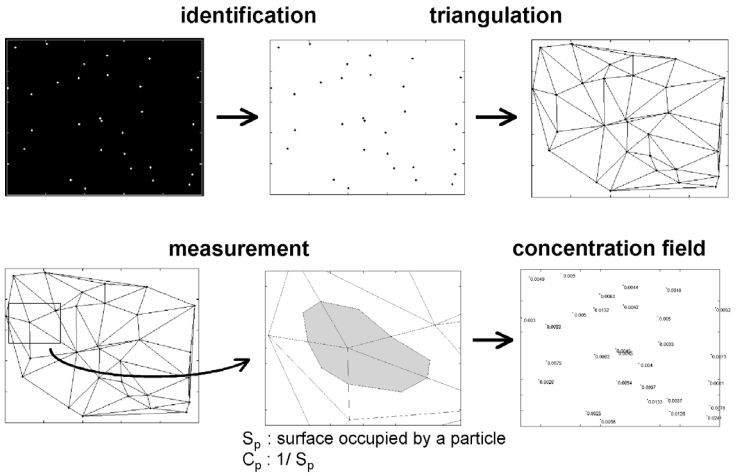

Figure 16: concentration measurement by triangulation

Hence, the concentration field is obtained on an unstructured mesh but it is easy to redistribute the information to a structured grid applying high order finite element method and using the same triangulation. The advantage of this approach is that the dynamic range is no more limited by the discrete nature of the recorded images since the particle position can be evaluated using sub-pixel interpolation and then the measured areas are not stacked to

discrete values. Nevertheless, the pixel-locking effect affecting the measurement of the particle position has to be also accounted for. Further analysis should be held to characterize this approach in a systematic way.

5.Conclusion

An extension of hybrid PIV-PTV method is presented. This tool initially dedicated to velocity measurement is used to measure simultaneous particle concentration field. A method based on particle counting is investigated and characterized.

The discrete nature of the recorded images leads to a coupling between the dynamic range (and then the accuracy) and the spatial resolution of the measurement. A trade-off has to be made between these two quantities. Systematic tests on synthetic images and real images as well showed that the tool has a non-linear response. Nevertheless, the mean measurements present self-similar profile and a correction is possible if experimental parameter such as the particle image diameter are determined. The instantaneous measurements are more delicate. They present scatter due to the limitation in the performances of identification algorithm and the error made on the particle position. Therefore, efforts have to be done towards the image processing methods to extract and to localize accurately the tracers. It was showed that using large interrogation windows attenuates this scatter but lowers the spatial resolution. The use of high-resolution camera is needed.

Another approach to analyze the spatial distribution of particles was proposed: the triangulation method. Further work will be made to further develop the theoretical investigation and to perform experimental applications to show the interest and to validate the tool.

Acknowledgement

The FRIA (Fonds pour la formation à la Recherche dans l'Industrie et l'Agriculture) and the FNRS (Fonds National pour la Recherche Scientifique) are gratefully acknowledged by the first author for their financial support. The contribution to this work of Deszö G. and Van Beeck J. is also appreciated (VKI).

References

Carosone F., Cenedese A., Querzoli G. (1995), Recognition of partially overlapped particles using the Kohonen neural network, Experiments in Fluids, Vol. 19, pp. 225 – 232

Etoh T., Takehara K., Okamoto K. (1998), The particle mask correlation method, Proceedings of the 8th Symposium on Flow Visualisation, Sorrento (Italy), Sept. 1-4

Guezennec Y.G., Kiritsis N. (1990), Statistical investigation of errors in particle image velocimetry, Experiments in Fluids, Vol. 10, pp. 138 – 146

Stitou A. and Riethmuller M.L. (2000), Extension of PIV to Super Resolution using PTV, Measurement Science Technology, accepted for publication in may 2001

van de Hulst (1957), Light scattering by small particles, Ed. John Wiley & Sons Inc., New York (republished 1981 by Dover publications, New York)

Zimmer L., Buchlin J-M., Riethmuller M.L (1999), Particle Tracking Velocimetry and Sizing: Application to liquid sprays, Proceedings of the International Workshop on Particle Image Velocimetry, Santa-Barbara (USA), Sept. 16-18

Westerweel J. (2000), Laser Induced Fluorescence from Particle Image Velocimetry and Associated techniques, edited by Riethmuller M.L., von Karman Institute Lecture Series, VKI LS 2000-01

ANNEXES

Annex 1: probability density function of presence of a particle with the effect of the error on the measurement of its position

We consider a window (area = w_s by w_s pixel^2) and a particle located inside this region (fig A-1). The measurement of this position is affected by a non-biased gaussian noise characterized by σ_{xe}. We assume first consider a one-dimensional situation and then we will extend it to two dimensions.

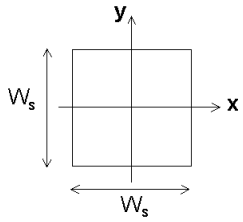

Fig A-1: referential adopted for the further calculations

We have $x_m = x_p + x_e$ with: x_m the measured position of the particle
x_p the real position
x_e the measurement error on the position

These values are modelised by the following probability density functions and an example is depicted in fig A-2.

$$\mathrm{pdf}(x_p) = \begin{cases} \dfrac{1}{w_s} & \text{if } |x_p| < \dfrac{w_s}{2} \\ 0 & \text{otherwise} \end{cases} \qquad \mathrm{pdf}(x_e) = \frac{1}{\sigma_{xe}\sqrt{2\Pi}}.\exp\left(-\frac{x_e^2}{2\sigma_{xe}^2}\right)$$

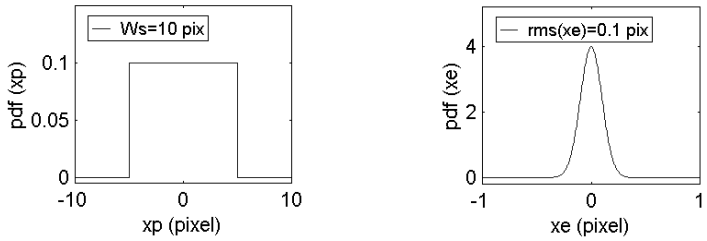

Fig A-2: pdf of position of a particle within a window and the measurement error of this position

The probability of localizing a particle at a point of interest x_m can be determined easily:

$$\begin{aligned} P(\text{localize a particle in } x_m) &= \sum_i P\left[\left(\text{particle}_i \text{ is lying in } x_p\right) \text{and} \left(\text{error } x_e = x_m - x_p\right)\right] \\ &= \sum_i P\left(\text{particle}_i \text{ is lying in } x_p\right).P\left(\text{error } x_e = x_m - x_p\right) \end{aligned}$$

Going to an integral form, it comes:

$$P(x_m) = \int_{-\frac{w_s}{2}}^{\frac{w_s}{2}} \left(\frac{1}{w_s}\right)\left(\frac{1}{\sigma_{xe}.\sqrt{2\Pi}}.\exp\left(-\frac{(x_m - x_p)^2}{2.\sigma_{xe}^{\ 2}}\right)\right).dx_p$$

$$= \left(\frac{1}{w_s.\sigma_{xe}.\sqrt{2\Pi}}\right)\left[\int_0^{\frac{w_s}{2}} \exp\left(-\frac{(x_m - x_p)^2}{2.\sigma_{xe}^{\ 2}}\right).dx_p - \int_0^{-\frac{w_s}{2}} \exp\left(-\frac{(x_m - x_p)^2}{2.\sigma_{xe}^{\ 2}}\right).dx_p\right]$$

$$= \left(\frac{1}{w_s.\sqrt{\Pi}}\right)\left[-\int_0^{\frac{x_m - \frac{w_s}{2}}{\sqrt{2}.\sigma_{xe}}} \exp(-u^2).du + \int_0^{\frac{x_m + \frac{w_s}{2}}{\sqrt{2}.\sigma_{xe}}} \exp(-v^2).dv\right] \qquad \text{with : } u = \frac{x_m - x_p}{\sqrt{2}.\sigma_{xe}} \quad , \quad v = \frac{x_m + x_p}{\sqrt{2}.\sigma_{xe}}$$

$$P(x_m) = \left(\frac{1}{2.w_s}\right).\left[\operatorname{erf}\left(\frac{x_m+\frac{w_s}{2}}{\sqrt{2}.\sigma_{xe}}\right)-\operatorname{erf}\left(\frac{x_m-\frac{w_s}{2}}{\sqrt{2}.\sigma_{xe}}\right)\right] \quad (xx) \qquad \text{with :} \quad \operatorname{erf}(z)=\frac{2}{\sqrt{\Pi}}.\int_0^z \exp(-t^2).dt$$

This equation expresses the probability distribution of presence of a particle. Examples of application are showed in fig A-3. it is also checked that:

$$\int_{-\infty}^{+\infty} P(x_m).dx_m = 1$$

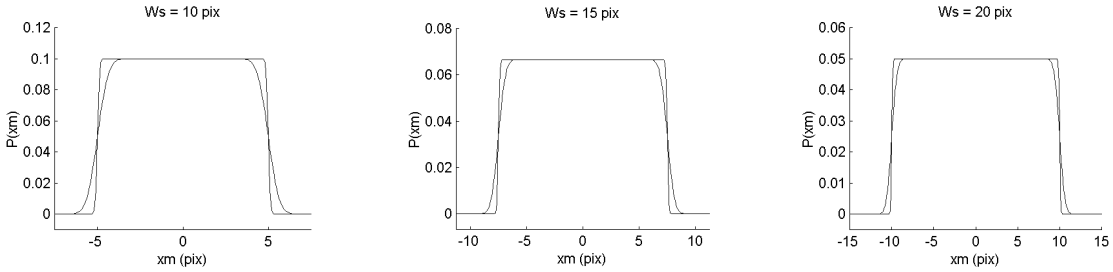

fig A-3 : probability distribution of presence of a measured particle for different window size and for 2 position error (σ_{xe}=0.1 pix and σ_{xe}=0.5 pix)

Then, the probability to localize an identified particle of a window of interest inside this region (P_{in}) is computed from the probability distribution of presence of such particle.

$$P_{in} = \int_{-\frac{w_s}{2}}^{\frac{w_s}{2}} P(x_m).dx_m = \int_{-\frac{w_s}{2}}^{\frac{w_s}{2}} \left(\frac{1}{2.w_s}\right).\left[\operatorname{erf}\left(\frac{x_m+\frac{w_s}{2}}{\sqrt{2}.\sigma_{xe}}\right)-\operatorname{erf}\left(\frac{x_m-\frac{w_s}{2}}{\sqrt{2}.\sigma_{xe}}\right)\right].dx_m$$

$$= \frac{\sqrt{2}}{2}.\frac{1}{\left(\frac{w_s}{\sigma_{xe}}\right)}.\left[\left(\int_0^{\frac{w_s}{\sqrt{2}.\sigma_{xe}}} \operatorname{erf}(u).du\right)-\left(\int_{-\frac{w_s}{\sqrt{2}.\sigma_{xe}}}^{0} \operatorname{erf}(v).dv\right)\right] \qquad \text{with :} \quad u=\frac{x_m+\frac{w_s}{2}}{\sqrt{2}.\sigma_{xe}} \quad , \quad v=\frac{x_m-\frac{w_s}{2}}{\sqrt{2}.\sigma_{xe}}$$

$$P_{in} = \frac{\sqrt{2}}{\left(\frac{w_s}{\sigma_{xe}}\right)}.\left[\frac{1}{\sqrt{2}}.\left(\frac{w_s}{\sigma_{xe}}\right).\operatorname{erf}\left(\frac{1}{\sqrt{2}}.\frac{w_s}{\sigma_{xe}}\right)+\frac{1}{\sqrt{\Pi}}.\exp\left(\frac{1}{2}.\left(\frac{w_s}{\sigma_{xe}}\right)^2\right)-\frac{1}{\sqrt{\Pi}}\right] \qquad \text{with :} \quad \int \operatorname{erf}(z).dz = z.\operatorname{erf}(z)+\frac{\exp(-z^2)}{\sqrt{\Pi}}$$

If we generalize to the two-dimensional situation by squaring the previous equation, we obtain:

$$P_{in} = \frac{2}{\left(\frac{w_s}{\sigma_{xe}}\right)^2}.\left[\frac{1}{\sqrt{2}}.\left(\frac{w_s}{\sigma_{xe}}\right).\operatorname{erf}\left(\frac{1}{\sqrt{2}}.\frac{w_s}{\sigma_{xe}}\right)+\frac{1}{\sqrt{\Pi}}.\exp\left(\frac{1}{2}.\left(\frac{w_s}{\sigma_{xe}}\right)^2\right)-\frac{1}{\sqrt{\Pi}}\right]^2$$

$$P_{out} = 1-\frac{2}{\left(\frac{w_s}{\sigma_{xe}}\right)^2}.\left[\frac{1}{\sqrt{2}}.\left(\frac{w_s}{\sigma_{xe}}\right).\operatorname{erf}\left(\frac{1}{\sqrt{2}}.\frac{w_s}{\sigma_{xe}}\right)+\frac{1}{\sqrt{\Pi}}.\exp\left(\frac{1}{2}.\left(\frac{w_s}{\sigma_{xe}}\right)^2\right)-\frac{1}{\sqrt{\Pi}}\right]^2$$

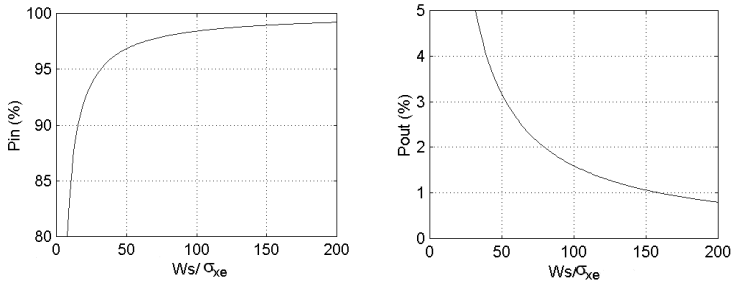

Fig A-4: probability for a particle to be localized inside/outside the window where it lies

Annex 2: probability of localizing a particle in a neighbouring window to the window where it lies

We compute here the probability that a particle is localized outside the window where it lies. Successively two situations are considered and are depicted in fig A-5: the particle of interest is moving by the side and by the corners of the windows and lies in a neighboring window.

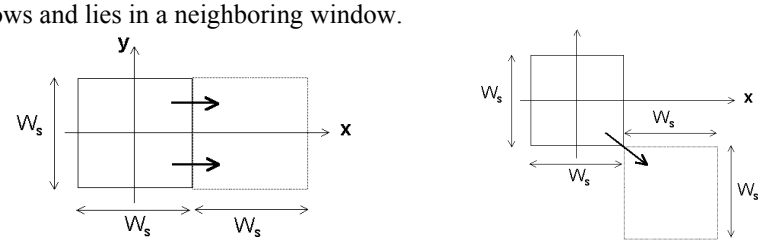

Fig A-5: particle localized outside the window where it lies (considered situation)

From the calculation done in Annex 1, we can write:

$$P_{side} = P_{in}.\int_{\frac{w_s}{2}}^{\frac{3w_s}{2}} P(x_m).dx_m = P_{in}.\int_{\frac{w_s}{2}}^{\frac{3w_s}{2}} \left(\frac{1}{2.w_s}\right).\left[\operatorname{erf}\left(\frac{x_m+\frac{w_s}{2}}{\sqrt{2}.\sigma_{xe}}\right)-\operatorname{erf}\left(\frac{x_m-\frac{w_s}{2}}{\sqrt{2}.\sigma_{xe}}\right)\right].dx_m$$

$$= P_{in}.\left(\frac{\sqrt{2}}{2}\right).\frac{1}{\left(\frac{w_s}{\sigma_{xe}}\right)}.\left[\left(\int_{\frac{w_s}{\sqrt{2}.\sigma_{xe}}}^{\frac{\sqrt{2}.w_s}{\sigma_{xe}}} \operatorname{erf}(u).du\right)-\left(\int_{0}^{\frac{w_s}{\sqrt{2}.\sigma_{xe}}} \operatorname{erf}(v).dx_m\right)\right]$$

$$= P_{in}.\left(\frac{\sqrt{2}}{2}\right).\frac{1}{\left(\frac{w_s}{\sigma_{xe}}\right)}.\left\{\sqrt{2}.\left(\frac{w_s}{\sigma_{xe}}\right).\left[\operatorname{erf}\left(\sqrt{2}.\frac{w_s}{\sigma_{xe}}\right)-\operatorname{erf}\left(\frac{\sqrt{2}}{2}.\frac{w_s}{\sigma_{xe}}\right)\right]+\frac{1}{\sqrt{\Pi}}.\left[\exp\left(-2.\left(\frac{w_s}{\sigma_{xe}}\right)^2\right)-2\exp\left(-\frac{1}{2}.\left(\frac{w_s}{\sigma_{xe}}\right)^2\right)+1\right]\right\}$$

$$P_{side} = \frac{1}{\left(\frac{w_s}{\sigma_{xe}}\right)^2}.\left[\frac{\sqrt{2}}{2}.\left(\frac{w_s}{\sigma_{xe}}\right).\operatorname{erf}\left(\frac{\sqrt{2}}{2}.\frac{w_s}{\sigma_{xe}}\right)+\frac{1}{\sqrt{\Pi}}.\exp\left(-\frac{1}{2}.\left(\frac{w_s}{\sigma_{xe}}\right)^2\right)-\frac{1}{\sqrt{\Pi}}\right]$$

$$.\left\{\sqrt{2}.\left(\frac{w_s}{\sigma_{xe}}\right).\left[\operatorname{erf}\left(\sqrt{2}.\frac{w_s}{\sigma_{xe}}\right)-\operatorname{erf}\left(\frac{\sqrt{2}}{2}.\frac{w_s}{\sigma_{xe}}\right)\right]+\frac{1}{\sqrt{\Pi}}.\left[\exp\left(-2.\left(\frac{w_s}{\sigma_{xe}}\right)^2\right)-2\exp\left(-\frac{1}{2}.\left(\frac{w_s}{\sigma_{xe}}\right)^2\right)+1\right]\right\}$$

and: $$P_{corner} = \left(\int_{\frac{w_s}{2}}^{\frac{3w_s}{2}} P(x_m).dx_m\right)^2$$

The previous calculations can then be used and we get:

$$P_{corner} = \frac{1}{2}.\frac{1}{\left(\frac{w_s}{\sigma_{xe}}\right)^2}.\left\{\sqrt{2}.\left(\frac{w_s}{\sigma_{xe}}\right).\left[\operatorname{erf}\left(\sqrt{2}.\frac{w_s}{\sigma_{xe}}\right)-\operatorname{erf}\left(\frac{\sqrt{2}}{2}.\frac{w_s}{\sigma_{xe}}\right)\right]+\frac{1}{\sqrt{\Pi}}.\left[\exp\left(-2.\left(\frac{w_s}{\sigma_{xe}}\right)^2\right)-2\exp\left(-\frac{1}{2}.\left(\frac{w_s}{\sigma_{xe}}\right)^2\right)+1\right]\right\}^2$$

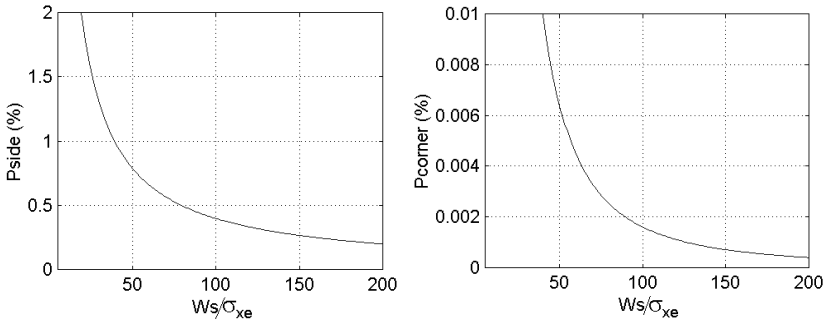

Fig A-6: probability of finding a particle in a neighboring window